Contactless characterization of the elastic properties of glass microspheres

Jérémie Maire, Tomasz Necio, Emigdio Chávez-Ángel, Martín Colombano, Juliana Jaramillo-Fernández, Clivia Sotomayor-Torres, Nestor Capuj, Daniel Navarro-Urrios

APL Materials

RESEARCH ARTICLE | APRIL 25 2023

Contactless characterization of the elastic properties of glass microspheres

Jeremie Maire ; Tomasz Necio ; Emigdio Chávez-Ángel ; Martín F. Colombano; Juliana Jaramillo-Fernández ; Clivia M. Sotomayor-Torres ; Nestor E. Capuj; Daniel Navarro-Urrios

APL Mater. 11, 041128 (2023)
https://doi.org/10.1063/5.0146969

Contactless characterization of the elastic properties of glass microspheres

Cite as: APL Mater. 11, 041128 (2023); doi: 10.1063/5.0146969
Submitted: 17 February 2023 • Accepted: 7 April 2023 •
Published Online: 25 April 2023

Jeremie Maire,[1,a] Tomasz Necio,[1] Emigdio Chávez-Ángel,[1] Martín F. Colombano,[2] Juliana Jaramillo-Fernández,[3] Clivia M. Sotomayor-Torres,[1,4] Nestor E. Capuj,[5,6] and Daniel Navarro-Urrios[3,b]

AFFILIATIONS

[1] Catalan Institute of Nanoscience and Nanotechnology (ICN2), CSIC and BIST, Campus UAB, Bellaterra 08193, Barcelona, Spain
[2] Université Paris Cité, CNRS, Laboratoire Matériaux et Phénomènes Quantiques, 75013 Paris, France
[3] MIND-IN2UB, Departament d'Electrònica, Facultat de Física, Universitat de Barcelona, Martí i Franquès 1 08028, Barcelona, Spain
[4] ICREA—Institució Catalana de Recerca i Estudis Avançats, Barcelona 08010, Spain
[5] Depto. Física, Universidad de La Laguna, 38200 San Cristóbal de La Laguna, Spain
[6] Instituto Universitario de Materiales y Nanotecnología, Universidad de La Laguna, 38071 Santa Cruz de Tenerife, Spain

[a] **Current address:** Univ. Bordeaux, CNRS, Bordeaux INP, I2M, UMR 5295, F-33400 Talence, France and YaaaArts et Metiers Institute of Technology, CNRS, Bordeaux INP, Hesam Universite, I2M, UMR 5295, F-33400 Talence, France.
[b] **Author to whom correspondence should be addressed:** dnavarro@ub.edu

ABSTRACT

Glass microspheres are of great interest for numerous industrial, biomedical, or standalone applications, but it remains challenging to evaluate their elastic and optical properties in a non-destructive way. In this work, we address this issue by using two complementary contactless techniques to obtain elastic and optical constants of glass microspheres with diameters ranging from 10 to 60 μm. The first technique we employ is Brillouin Light Scattering, which yields scattering with longitudinal acoustic phonons, the frequency of which is found to be 5% lower than that measured in the bulk material. The second technique involves exciting the optical whispering gallery modes of the microspheres, which allows us to transduce some of their vibrational modes. The combined data allow for extracting the refractive index and the elastic constants of the material. Our findings indicate that the values of those properties are reduced with respect to their bulk material counterpart due to an effective decrease of the density, resulting from the fabrication process. We propose the use of this combined method to extract elastic and optical parameters of glass materials in microsphere geometries and compare them with the values of the pristine material from which they are formed.

INTRODUCTION

High quality spherical microspheres are one of the earliest forms of optical microcavities, and, as such, they have been widely studied and utilized for a variety of applications, such as sensing,[1–3] magnetometry,[4] or optomechanical oscillators.[5,6] In this context, light is confined inside the microcavity via total internal reflection, therefore, leading to whispering gallery modes resonances.[7] These resonances can lead, for instance, to a strong enhancement of the spontaneous emission rate in light emitting media.[8] The microsphere shape itself has also been used to demonstrate low intermolecular binding detection limits for biosensing applications,[1] ultrahigh optical quality factors,[9] optical lasing at low pump power thresholds,[10] and even mechanical lasing.[6] Microspheres can also be exploited in the form of colloidal crystals with applications in the fields of organic electronics, photonics, phononics,[11,12] lithography,[13] and thermal management.[14–16] They can be produced in a variety of materials, such as polymers, crystalline and glassy compounds, and sizes ranging from a few hundred nanometers to millimeters. They can be easily fabricated, either individually or in large quantities by a variety of methods, which include polishing, chemical etching, and rapid quenching of liquid droplets. Their

elastic properties are of crucial importance for most applications. For example, in phononic colloidal crystals, the phonon dispersion relation is directly dependent on the elastic properties of the spheres as well as on their size.[11,17] In composite materials, spheres can be added to reinforce mechanically a matrix,[18] requiring precise characterization of their elastic properties. However, it is well known that in many cases, the fabrication method can significantly alter the optical and elastic properties of the material in the microsphere shape with respect to the bulk values. Extracting these properties below the millimeter scale without damaging the spheres remains a challenge.

Here, we combine two optical non-destructive techniques, namely, inelastic Brillouin light scattering (BLS) and optomechanical coupling (OM), to extract the elastic and optical constants of Barium–Titanium-Silicate glass material in a microsphere with diameters ranging from 10 to 60 μm. We have observed that the longitudinal phonon frequencies detected in the BLS experiment decrease in the microsphere when compared to those measured in the pristine bulk material by as much as 5%; information that is considered alone can be attributed either to a reduction of the material refractive index, to a relaxation of the elastic properties, or a combination of both. The analysis of the frequency of the sphere vibrational modes detected with the OM technique allows extracting the elastic constants of the material in the microsphere in a reliable way, leading to longitudinal and transversal sound velocities that are 4957 m/s (2% less than the value extracted from the BLS measurement of the bulk material) and 2655 m/s. The material refractive index at 532 nm in the microsphere as extracted from the BLS experiment is thus 1.73, which is 3% lower than that of the bulk. This set of values also allows extracting an effective mass density value for the glass BTS material in the microsphere form of 4126 kg/m^3, which is about 8% lower than the bulk value. Thus, the experimental results indicate that the fabrication process induces an effective decrease in density, which explains the lowering in the refractive index and the elastic constants of the material.

SAMPLE FABRICATION

The Nd-doped Barium–Titanium-Silicate (BTS) microspheres with a composition of BaO(40%)–TiO_2(20%)–SiO_2(40%) and 1.5%$_{mol}$ Nd_2O_3 were fabricated by quenching liquid droplets. We first prepare a precursor by mixing and melting commercial powders of ACS reagent grade (purity ≥99.9%) $BaCO_3$, TiO_2, SiO_2, and Nd_2O_3 in a crucible at 1500 °C for one hour. The precursor is then crushed using a pestle and mortar to obtain particles close in size to the desired microspheres. These particles are then dropped through a vertical furnace and melt during the fall. The surface tension pulls them into spheres, which quench into an amorphous state when reaching the cooler region outside the furnace. With this method, microspheres with diameters D ranging from 10 to 100 μm are obtained. This method has been used before to fabricate microspheres, possessing optical modes with high quality factors[6,8] up to 10^8.[4] Its principle is explained in more detail elsewhere.[19] The density and refractive index of the bulk material are ρ = 4465 kg/m^3[20] and η = 1.78,[21] respectively.

RESULTS AND DISCUSSION

BLS and speed of sound

The sound velocity and the phonon frequency of the microspheres were determined from Brillouin light scattering (BLS) measurements. BLS is a widely used technique for measuring sound velocities and acoustic phonon frequencies in solids, liquids, and gases.[22–25] It probes the light frequency shift, resulting from the inelastic scattering of the light induced by thermally populated acoustic waves in the medium. During this inelastic scattering process, the incident photon either loose or gain energy so that a phonon is emitted or absorbed. This results in the energy of inelastically backscattered photons shifting to lower (Stokes) or higher (Anti-Stokes) values, respectively. The difference between incident and backscattered photon energy corresponds to the phonon energy. To detect this shift of a few GHz, much smaller than that of Raman scattering, a six-pass tandem Fabry–Perot interferometer is widely used.[26]

More recently, BLS has been used to measure the dispersion relation in phononic crystals[27] and mechanical properties in microsphere-based colloidal crystals.[28] To that effect, the system was mounted with a microscope objective, enabling precise selection of the area and depth of material to be characterized, which is also adequate for measuring a single microsphere with diameters larger than a few micrometers. Our implementation comprises a 532 nm laser focused on a microsphere by means of a ×50 microscope objective (NA = 0.45). The position of the laser beam on the microsphere is adjusted by a two-axis translation stage. After being backscattered, the light is collected and directed toward a Tandem Fabry–Perot Interferometer.[29] This device consists of two Fabry–Perot cavities placed in series, each one of slightly different lengths, which allows for a very narrow bandwidth and a wide free spectral range. The mirrors on one side of each cavity oscillate with an amplitude of 490 nm around the position in resonance with the elastic peak, which, combined with the total length of the tandem cavity, determines the range of frequency shifts of the inelastically scattered light that can be detected. Each mirror's position scanned during the sweeps corresponds to a single frequency shift that is detected by a photodiode. The back-and-forth movement of the mirrors is then repeated thousands of times, and the photons counted at each frequency are summed to form the spectra. To minimize contamination of the signal by the substrate, the spheres were deposited on a flat surface and illuminated by the excitation laser from the side. A schematic representation of the configuration is shown in Fig. 1(a). An optical microscope image of a sphere is shown in the inset of Fig. 1(a). The measurements are performed at ambient temperature in the air. The extremely strong signal at the origin of the spectrum [leftmost part of Fig. 1(b)] corresponds to elastic light scattering. Both Stokes (negative frequency shift) and Anti-Stokes peaks (positive frequency shift) are fitted with a Lorentzian function. An average of their peak position is used to compensate for the slight asymmetry of the spectrum with respect to the laser wavelength, which is due to the non-perfect tuning of the Fabry–Perot interferometer. The experimental error in determining the frequencies, including the Lorentz peak fitting, remains below 0.6%. Figure 1(b) shows representative Brillouin spectra fitted with the Lorentzian. In

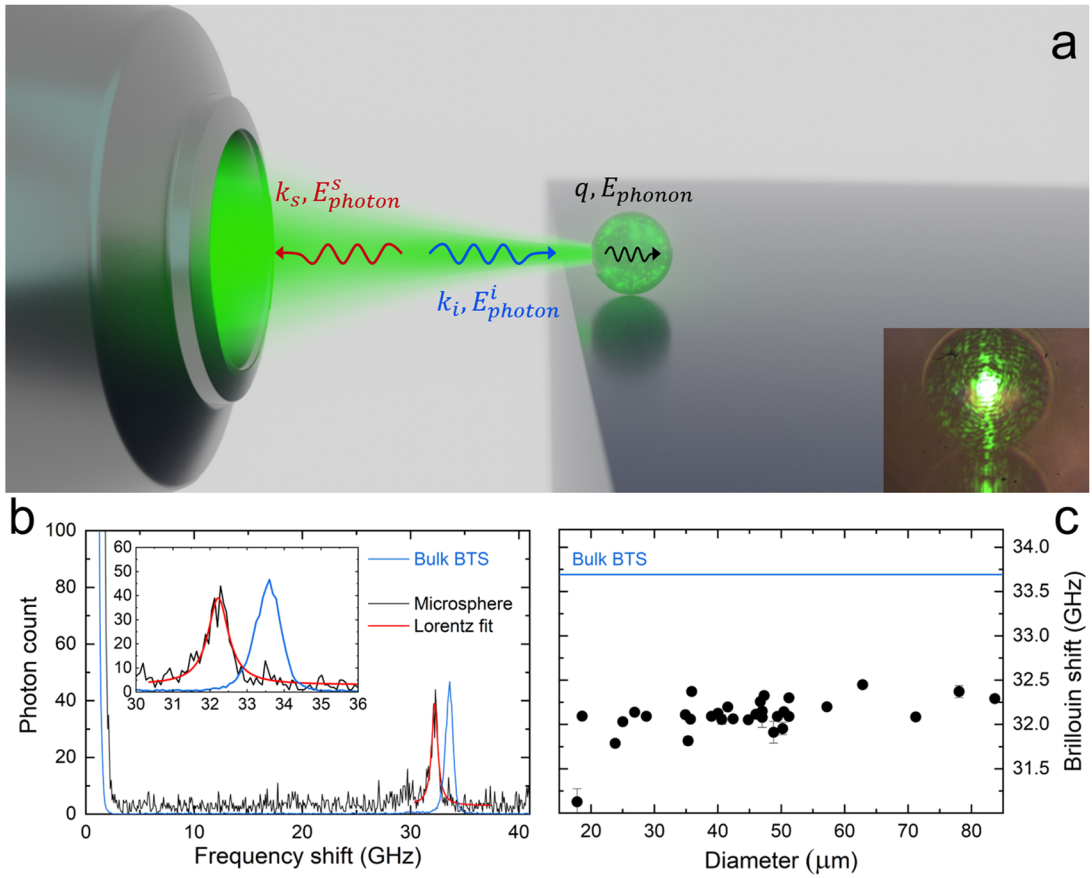

FIG. 1. BLS of microspheres. (a) Light with energy E^i_{photon} is focused on the microsphere and excites acoustic waves in the microsphere of energy E_{phonon}. Scattered light of energy E^s_{photon} is then collected by the same microscope objective and sent to be detected (see main text). Brillouin frequency shift doublet is defined as $f = \pm E_{phonon}/h = (E^i_{photon} - E^s_{photon})/h$, where h is the Planck constant. The acoustic wave vector q is selected geometrically and has a magnitude of $\pm q = k_s - k_i$. Symbols k_i, k_s, and q denote the incident light, scattered light, and phonon wave vectors, respectively. (Inset) Optical microscope image of the microsphere obtained with a ×50 objective. The green light corresponds to the laser used for the experiment. (b) Typical BLS spectra for bulk BTS (blue line) and a microsphere (black line). For comparison, the signal for bulk is scaled down by a factor of ×20. The red curve corresponds to a Lorentzian fit to the peak associated with the microsphere. Only the anti-stokes part of the spectra is shown for clarity. (Inset) Close-up view of the region with the Brillouin peaks. (c) Brillouin shift as a function of the diameter.

the backscattering geometry, the selection rules favor the longitudinal mode, and unless significant light depolarization occurs, no coupling with the acoustic shear modes takes place.[30]

In the backscattering configuration, the Brillouin shift is related to the frequency of the scattering acoustic wave through the following expression:

$$f_{BLS} = \frac{2 \cdot \eta \cdot v_{long}}{\lambda}, \tag{1}$$

where v_{long} is the speed of longitudinal sound waves in the material, λ is the photon wavelength (532 nm), and η is the refractive index of the material at that wavelength. Figure 1(c) shows the Brillouin shift as a function of sphere diameter. We note a clear difference between bulk BTS and microspheres, with a smaller frequency detected in the microspheres independently of their diameter, which corresponds to a 5% difference. The error bars consider the error in the Lorentz fit, as well as the error during the measurement of the spectrum. If we consider the refractive index of the bulk material given above, then we can calculate the speed of longitudinal sound waves for the bulk material, which is, therefore, $v_{long,BTS} = 5036$ m/s.

The decrease in phonon frequency as measured by BLS may result from a reduction in elastic constants or the refractive index of the material at 532 nm or both. However, from this set of data alone, it is not possible to isolate each contribution. Therefore, a complementary technique based on the OM coupling of optical and vibrational modes of the microspheres has been used to determine the physical origin of the phonon frequency shift observed in BLS.

MECHANICAL MODE

The determination of the elastic properties of the material is achieved through the analysis of the vibrational eigenmodes of the

microspheres, commonly referred to as the Lamb modes. The Lamb modes were measured using the experimental setup sketched in Fig. 2(a), which is based on the coupling of evanescent light from a tapered fiber to the whispering gallery modes of the spheres.[6] An infrared driving laser with tunable wavelength (1440–1640 nm) and power up to 20 mW passes through a polarization controller before being coupled to a tapered microlooped fiber. The microloop is then positioned in contact with the microsphere as shown in the microscope image in Fig. 2(a). When the laser wavelength matches an optical resonance of the microsphere, the mechanical modes activated by the thermal Langevin force modulate the transmission of the tapered fiber around its static value. The transmitted signal is then detected by a 12 GHz bandwidth InGaAs detector connected to a signal analyzer with a bandwidth of 13.5 GHz. Similarly to the BLS experiments, OM measurements are performed at room temperature and atmospheric pressure.

With the evanescent fiber coupling system, we first acquire an optical transmission spectrum [see Fig. 2(b)] in which each sharp dip corresponds to an optical resonance. Details about optical resonances in these microspheres are given elsewhere.[6] The mechanical spectrum is obtained by processing the transmitted optical signal with a spectrum analyzer. In that spectrum, the thermal motion of vibrational modes with a large enough degree of OM coupling appears as Lorentzian peaks with quality factors limited to around

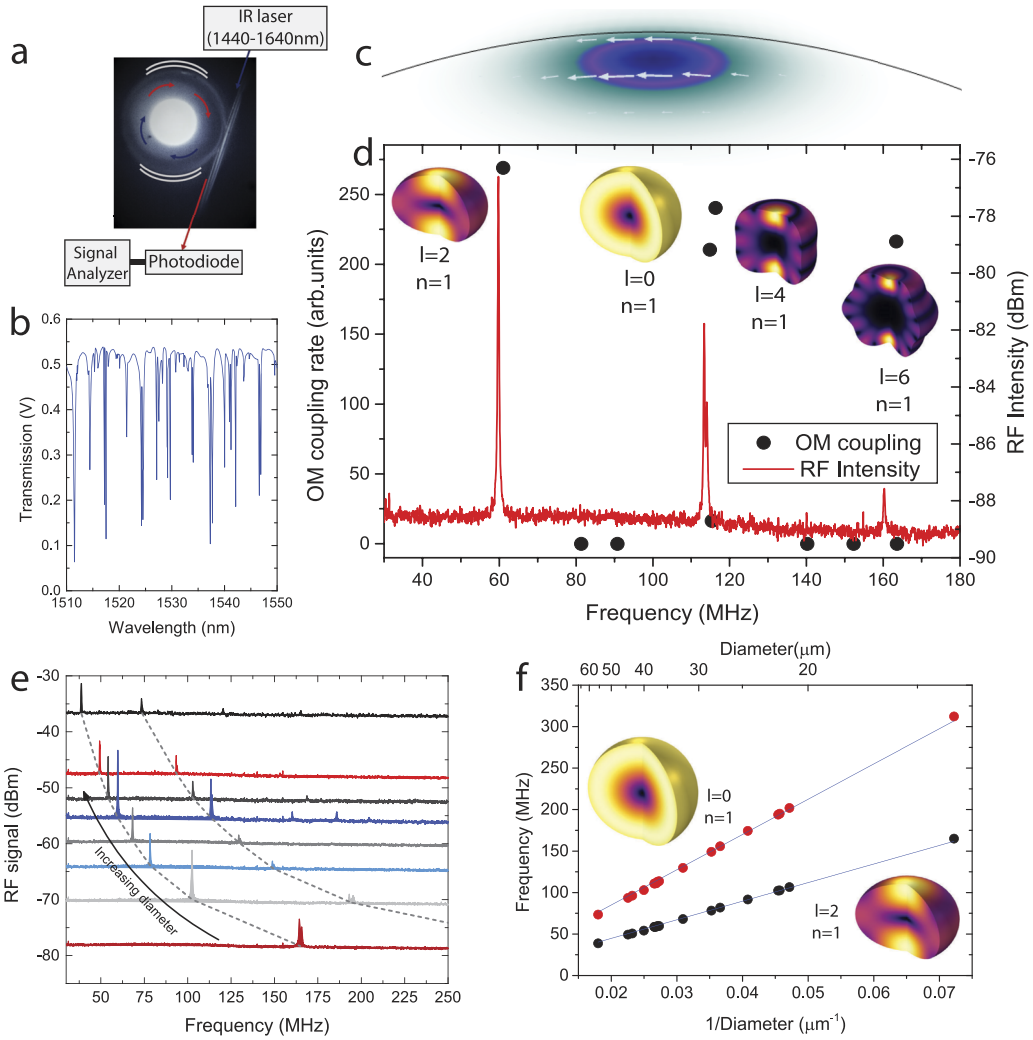

FIG. 2. Optomechanical study of microspheres. (a) Schematic of the evanescent fiber coupling measurement system. The picture is a microscope image of a microsphere with the tapered fiber aligned. (b) Optical spectrum of a microsphere as measured by the IR detector. (c) Simulated optical whispering gallery mode at 1530 nm for a microsphere of diameter 36.6 μm. The white arrows indicate the direction of the electric field. (d) Radio frequency (RF) spectra of a microsphere of diameter D = 36.6 μm (red curve) and simulated optomechanical coupling rate with vibrational modes of the sphere. (e) RF spectra of microspheres of different diameters. The vertical offset represents the increase in diameter. The dashed gray lines are guides for the eyes for the two first modes. (f) Frequencies of the two first modes of each sphere as a function of the inverse of the diameter, where the lines are linear fits to the data. The color schemes represent the electric field in panel c and the deformation in panels d and f.

100. The red curve of Fig. 2(d) shows a representative example of the registered mechanical spectra that corresponds to a sphere of diameter D = 36.6 μm. Several peaks are visible, which correspond to several vibrational modes of the spheres.

Finite element methods simulations computed with COMSOL Multiphysics are used to identify which of the vibrational modes supported by the microsphere can be detected in the experiment, i.e., can display enough degree of OM coupling with the optical whispering gallery modes to overcome the noise level. Figure 2(c) illustrates the optical mode of a sphere that has been used to perform the simulations, which is a fundamental WGM with azimuthal polarization emphasized by the white arrows. It should be noted that comparable results can be achieved using other optical modes. We then computed all the vibrational modes of the microsphere in the frequency range of the experiment and finally calculated the optomechanical coupling considering only the moving boundary contribution.[31] The results are shown as black dots in Fig. 2(d), allowing us to conclude that the observed vibration modes are essential of the second class (spheroidal) type,[32] which are univocally described by the angular momentum index (l) and the overtone number (n).[33] In the spheroidal type of modes, the sphere expands and contracts along its radial axis, with the lower frequency mode having l = 2 sometimes called "American football" mode and the second mode fulfilling l = 0, which corresponds with the "breathing" mode of the sphere. It is worth noting that the fundamental mode with l = 4 appears very close to the breathing mode.

Figure 2(e) shows the mechanical spectra of spheres with increasing diameter, from bottom to top, respectively. We observe that the frequency of each mechanical mode decreases with the increasing diameter of the sphere. In Fig. 2(f), we plot the value of the mechanical frequency as a function of 1/D for the l = 2 and l = 0 vibrational modes. The apparent fitting using a straight line provides a slope of $\beta_{l=2}$ = 2233 m/s and $\beta_{l=0}$ = 4210 m/s, respectively, which can be understood as a normalized eigenfrequency. The analytical calculation of the vibrational eigenmodes of elastic isotopic spheres indeed shows a dependence of mode frequencies proportional to $1/D$ in the absence of geometrical stress effects in the microspheres, so we can conclude that the elastic properties of the material composing the microspheres do not depend on their diameter. The frequency of the vibrational modes of the spheroidal type is calculated by finding the roots of the following equation valid for l > 0:[32,34]

$$
\begin{aligned}
&-\frac{1}{2}\left(\frac{\beta_l}{2v_{trans}}\right)^2\left(2l^2-l-1-\frac{1}{2}\left(\frac{\beta_l}{2v_{trans}}\right)^2\right)j_l\left(\frac{\beta_l}{2v_{long}}\right)j_l\left(\frac{\beta_l}{2v_{trans}}\right)\\
&+\left(l^3+2l^2-l-2-\left(\frac{\beta_l}{2v_{trans}}\right)^2\right)\left(\frac{\beta_l}{2v_{long}}\right)j_{l+1}\left(\frac{\beta_l}{2v_{long}}\right)j_l\left(\frac{\beta_l}{2v_{trans}}\right)\\
&+\left(l^3+l^2-2l-\frac{1}{2}\left(\frac{\beta_l}{2v_{trans}}\right)^2\right)\left(\frac{\beta_l}{2v_{trans}}\right)j_l\left(\frac{\beta_l}{2v_{long}}\right)j_{l+1}\left(\frac{\beta_l}{2v_{trans}}\right)\\
&+\left(2-l^2-l\right)\left(\frac{\beta_l^2}{4v_{trans}v_{long}}\right)j_{l+1}\left(\frac{\beta_l}{2v_{long}}\right)j_{l+1}\left(\frac{\beta_l}{2v_{trans}}\right)=0, \qquad (2)
\end{aligned}
$$

where j_l are the spherical Bessel functions of the first kind and v_{trans} is the transversal sound velocity.

In the case of l = 0, the correct equation to use is[35]

$$\tan\left(\frac{\beta_{l=0}}{2v_{long}}\right)-\frac{\beta_{l=0}}{2v_{long}}\left(1-\frac{1}{4}\left(\frac{\beta_{l=0}}{2v_{trans}}\right)^2\right)^{-1}=0. \qquad (3)$$

When the experimental values of $\beta_{l=2}$ and $\beta_{l=0}$ are plugged into Eqs. (2) and (3), respectively, the resulting solutions are the (v_{trans}, v_{long}) curves plotted in Fig. 3. The intersection of the two curves allows extracting the pair of values that are fitting both vibrational modes. In our case, we obtain v_{long} = 4957 m/s and v_{trans} = 2655 m/s. An equivalent analysis including the {l = 4, n = 1} and {l = 6, n = 1} vibrational modes is provided in the supplementary material S2, where we verify the model since the crossing point of the extracted {v_{long}, v_{trans}} curves is almost the same. The value of v_{long} is 2% lower than the value extracted from the BLS measurement of the bulk material. It is also worth noting that FEM simulations agree well with the OM experiment by using these pair of acoustic velocities as input material parameters [see Fig. 2(d)]. Since the acoustic velocities of the material within the spheres are accurately determined, it is then possible to extract the refractive index at λ = 532 nm from Eq. (1), which gives a value of η_{sph} = 1.733, i.e., 3% lower than that of the bulk material. Finally, we can use the well-known Newton–Drude formula[36,37] to extract the density ρ_{sph} of the material of the sphere,

$$\frac{(\eta^2-1)}{\rho_{sph}}=\frac{\alpha'}{W\varepsilon_o}, \qquad (4)$$

where the right-hand side is a constant that can be determined from the bulk values (α' is the mean molar polarizability, ε_o the dielectric permittivity, and W is the molecular weight). By substituting η_{sph} in Eq. (4), we get that the density is ρ_{sph} = 4126 kg/m^3, which is about 8% lower than the bulk value.

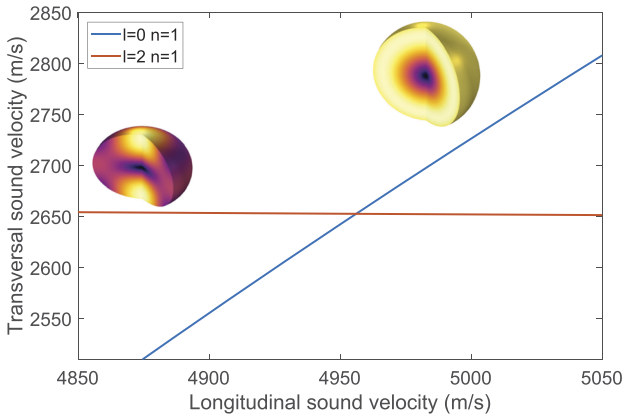

FIG. 3. Extraction of the elastic parameters. Transversal and longitudinal sound velocity curves that satisfy Eqs. (2) (orange curve) and (3) (blue curve) when including the experimental values of the vibrational frequencies. The blue curve corresponds to the {l = 0, n = 1} mode, and the orange curve corresponds to the {l = 2, n = 1} mode.

DISCUSSION ON THE ELASTIC AND OPTICAL PROPERTIES OF THE MICROSPHERES

The fabrication process used for the microspheres involves a thermal cycle that can directly affect the density of the resulting glass, which has been shown to directly depend on the quenching temperature and quenching rate, i.e., the cooling speed.[38] Due to the characteristics of the solidification process of the microsphere, we indeed expect the sphere to have a lower density, which we can estimate simply. When heated up and melted, the volume occupied by the material increases by $3 \times \alpha \times (T_{melt} - T_{init}) \approx 3\%$, where we have used the thermal expansion coefficient of the solid glass phase α, which is considered to be constant in the range of temperature used for the thermal treatment. T_{melt} is the temperature used to melt the chip, and T_{init} is the initial temperature. When cooling, the sphere will contract until the outermost layer reaches the glass transition temperature, at which temperature that layer will solidify. It is then possible to calculate an upper limit of the average density of the sphere material, which is smaller than that of the bulk material by at least 1.9%. It is important to note that the estimate provided is a conservative one, due to the existence of a temperature increase toward the center of the sphere and the fact that the expansion coefficient of melted glass can be significantly higher than that of its solid counterpart.[39]

CONCLUSIONS

In conclusion, we have used two non-destructive contactless optical techniques, namely, Brillouin Light Scattering and optomechanical evanescent coupling, to determine the elastic and optical properties of glass microspheres with diameters ranging from 10 to 60 μm. Our observations indicate that the Brillouin shift displayed by the microspheres is independent of sphere diameter and lower than that observed in the bulk material. This decrease has been quantitatively attributed to a reduction in the refractive index and the elastic constants of the material in the microsphere. All these material parameters have been univocally determined thanks to the independent extraction of the elastic constants of the material using the optomechanical coupling technique and fitting the experimental results to an analytical model of the vibrations of an elastic sphere. We attribute the observed changes with respect to the bulk material to a lower density in the spheres originating from the thermal treatment during the fabrication process, which is widely employed in the field. The advantage of our characterization method lies in its contactless nature and the wide range of spheres and materials that can be characterized. It is particularly useful for high Q-factor optical cavities without damaging them and can be adapted to other simple geometries.

SUPPLEMENTARY MATERIAL

The supplementary material file contains four sections and six figures: Section S1 contains a double check of the analytical model using finite-element-method simulations of the vibrational modes of the spheres. Section S2 repeats the analysis performed in the main text for the {l = 0, n = 1} and {l = 2, n = 1} vibrational modes and applies it to the {l = 4, n = 1} and {l = 6, n = 1} vibrational modes that are also visible in some of the RF spectra. This analysis verifies the accuracy of the method. Section S3 studies the linewidth of the Brillouin peaks as a function of the sphere diameter. Section S4 is dedicated to the analysis of the sphericity of the microscope using an image analysis technique.

ACKNOWLEDGMENTS

This work was supported by the MICINN projects ALLEGRO (Grant No. PID2021-124618NB-C22) and MOCCASIN-2D (Grant No. TED2021-132040B-C21). TN acknowledges the support of the European Commission through the Erasmus + program. J.M., E.C.A., M.F.C., and C.M.S.T. acknowledge the support of the Spanish projects S. Ochoa 2017-0706, MINECO Project No. FIS2015-70862-P, and the SGR Project No. SGR1238. J.M. and C.M.S.T. acknowledge support by the EC Future Emerging Technologies project Grant Agreement No. 753450 (PHENOMEN).

AUTHOR DECLARATIONS

Conflict of Interest

The authors have no conflicts to disclose.

Author Contributions

Jeremie Maire: Data curation (equal); Formal analysis (equal); Investigation (equal); Visualization (equal); Writing – original draft (equal); Writing – review & editing (equal). **Tomasz Necio**: Data curation (equal); Formal analysis (equal); Investigation (equal); Methodology (lead); Software (equal). **Emigdio Chávez-Ángel**: Investigation (supporting); Writing – review & editing (equal). **Martín F. Colombano**: Investigation (supporting); Software (equal). **Juliana Jaramillo-Fernández**: Investigation (equal); Writing – review & editing (equal). **Clivia M. Sotomayor-Torres**: Funding acquisition (equal); Project administration (equal). **Nestor E. Capuj**: Conceptualization (equal); Investigation (equal); Resources (lead). **Daniel Navarro-Urrios**: Conceptualization (equal); Data curation (equal); Formal analysis (equal); Funding acquisition (equal); Investigation (equal); Methodology (equal); Project administration (equal); Software (equal); Supervision (lead); Validation (equal); Visualization (equal); Writing – review & editing (equal).

DATA AVAILABILITY

The data that support the findings of this study are available from the corresponding author upon reasonable request.

REFERENCES

[1] F. Vollmer and S. Arnold, "Whispering-gallery-mode biosensing: Label-free detection down to single molecules," Nat. Methods **5**(7), 591–596 (2008).
[2] N. M. Hanumegowda, C. J. Stica, B. C. Patel, I. White, and X. Fan, "Refractometric sensors based on microsphere resonators," Appl. Phys. Lett. **87**(20), 201107 (2005).
[3] C.-H. Dong, L. He, Y.-F. Xiao, V. R. Gaddam, S. K. Ozdemir, Z.-F. Han, G.-C. Guo, and L. Yang, "Fabrication of high-Q polydimethylsiloxane optical microspheres for thermal sensing," Appl. Phys. Lett. **94**(23), 231119 (2009).

[4]M. F. Colombano, G. Arregui, F. Bonell, N. E. Capuj, E. Chavez-Angel, A. Pitanti, S. O. Valenzuela, C. M. Sotomayor-Torres, D. Navarro-Urrios, and M. V. Costache, "Ferromagnetic resonance assisted optomechanical magnetometer," Phys. Rev. Lett. **125**(14), 147201 (2020).
[5]G. Bahl, J. Zehnpfennig, M. Tomes, and T. Carmon, "Stimulated optomechanical excitation of surface acoustic waves in a microdevice," Nat. Commun. **2**(1), 403 (2011).
[6]A. Toncelli, N. E. Capuj, B. Garrido, M. Sledzinska, C. M. Sotomayor-Torres, A. Tredicucci, and D. Navarro-Urrios, "Mechanical oscillations in lasing microspheres," J. Appl. Phys. **122**(5), 053101 (2017).
[7]A. N. Oraevsky, "Whispering-gallery waves," Quantum Electron. **32**(5), 377 (2002).
[8]L. L. Martín, D. Navarro-Urrios, F. Ferrarese-Lupi, C. Pérez-Rodríguez, I. R. Martín, J. Montserrat, C. Domínguez, B. Garrido, and N. Capuj, "Laser emission in Nd^{3+} doped barium–titanium–silicate microspheres under continuous and chopped wave pumping in a non-coupled pumping scheme," Laser Phys. **23**(7), 075801 (2013).
[9]K. J. Vahala, "Optical microcavities," Nature **424**(6950), 839–846 (2003).
[10]G. S. Murugan, M. N. Zervas, Y. Panitchob, and J. S. Wilkinson, "Integrated Nd-doped borosilicate glass microsphere laser," Opt. Lett. **36**(1), 73–75 (2011).
[11]E. Alonso-Redondo, M. Schmitt, Z. Urbach, C. M. Hui, R. Sainidou, P. Rembert, K. Matyjaszewski, M. R. Bockstaller, and G. Fytas, "A new class of tunable hypersonic phononic crystals based on polymer-tethered colloids," Nat. Commun. **6**(1), 8309 (2015).
[12]T. Liu, S. Pihan, M. Roth, M. Retsch, U. Jonas, J. S. Gutmann, K. Koynov, H.-J. Butt, and R. Berger, "Frequency response of polymer films made from a precursor colloidal monolayer on a nanomechanical cantilever," Macromolecules **45**(2), 862–871 (2012).
[13]L. Isa, K. Kumar, M. Müller, J. Grolig, M. Textor, and E. Reimhult, "Particle lithography from colloidal self-assembly at liquid–liquid interfaces," ACS Nano **4**(10), 5665–5670 (2010).
[14]Y. Zhai, Y. Ma, S. N. David, D. Zhao, R. Lou, G. Tan, R. Yang, and X. Yin, "Scalable-manufactured randomized glass-polymer hybrid metamaterial for daytime radiative cooling," Science **355**(6329), 1062–1066 (2017).
[15]G. K. S. Khagokpam and S. Halder, "Paraffin wax microsphere embedded epoxy composites for potential thermal management in electronic devices," High Perform. Polym. **31**(7), 767–777 (2019).
[16]J. Jaramillo-Fernandez, G. L. Whitworth, J. A. Pariente, A. Blanco, P. D. Garcia, C. Lopez, and C. M. Sotomayor-Torres, "A self-assembled 2D thermofunctional material for radiative cooling," Small **15**(52), 1905290 (2019).
[17]W. Cheng, J. Wang, U. Jonas, G. Fytas, and N. Stefanou, "Observation and tuning of hypersonic bandgaps in colloidal crystals," Nat. Mater. **5**(10), 830–836 (2006).
[18]H.-B. Yao, H.-Y. Fang, X.-H. Wang, and S.-H. Yu, "Hierarchical assembly of micro-/nano-building blocks: Bio-inspired rigid structural functional materials," Chem. Soc. Rev. **40**(7), 3764–3785 (2011).
[19]G. R. Elliott, D. W. Hewak, G. S. Murugan, and J. S. Wilkinson, "Chalcogenide glass microspheres; their production, characterization and potential," Opt. Express **15**(26), 17542–17553 (2007).
[20]C. Shen, H. Zhang, H. Cong, H. Yu, J. Wang, and S. Zhang, "Investigations on the thermal and piezoelectric properties of fresnoite $Ba_2TiSi_2O_8$ single crystals," J. Appl. Phys. **116**(4), 044106 (2014).
[21]C. Shen, H. Zhang, D. Wang, J. Wang, and R. Boughton, "Optical properties of the fresnoite $Ba_2TiSi_2O_8$ single crystal," Crystals **7**(2), 53 (2017).
[22]J. G. Dil, "Brillouin scattering in condensed matter," Rep. Prog. Phys. **45**(3), 285 (1982).
[23]G. Benedek and T. Greytak, "Brillouin scattering in liquids," Proc. IEEE **53**(10), 1623–1629 (1965).
[24]T. Yogi, K. Sakai, and K. Takagi, "Light beating spectroscopy of Brillouin scattering in gases and solids," J. Appl. Phys. **100**(2), 023505 (2006).
[25]M. del R. Rodríguez-Laguna, A. Castro-Alvarez, M. Sledzinska, J. Maire, F. Costanzo, B. Ensing, M. Pruneda, P. Ordejón, C. M. S. Torres, and P. Gómez-Romero, "Mechanisms behind the enhancement of thermal properties of graphene nanofluids," Nanoscale **10**(32), 15402–15409 (2018).
[26]S. M. Lindsay, M. W. Anderson, and J. R. Sandercock, "Construction and alignment of a high performance multipass vernier tandem Fabry–Perot interferometer," Rev. Sci. Instrum. **52**(10), 1478–1486 (1981).
[27]B. Graczykowski, M. Sledzinska, N. Kehagias, F. Alzina, J. S. Reparaz, and C. M. Sotomayor Torres, "Hypersonic phonon propagation in one-dimensional surface phononic crystal," Appl. Phys. Lett. **104**(12), 123108 (2014).
[28]B. Graczykowski, N. Vogel, K. Bley, H.-J. Butt, and G. Fytas, "Multiband hypersound filtering in two-dimensional colloidal crystals: Adhesion, resonances, and periodicity," Nano Lett. **20**(3), 1883–1889 (2020).
[29]J. R. Sandercock, in *Light Scattering in Solids III: Recent Results*, edited by M. Cardona and G. Güntherodt (Springer Berlin Heidelberg, Berlin, Heidelberg, 1982), pp. 173–206.
[30]R. Vacher and L. Boyer, "Brillouin scattering: A tool for the measurement of elastic and photoelastic constants," Phys. Rev. B **6**(2), 639 (1972).
[31]S. G. Johnson, M. Ibanescu, M. A. Skorobogatiy, O. Weisberg, J. D. Joannopoulos, and Y. Fink, "Perturbation theory for Maxwell's equations with shifting material boundaries," Phys. Rev, E **65**(6), 66611 (2002).
[32]H. Lamb, "On the vibrations of an elastic sphere," Proc. London Math. Soc. **s1-13**(1), 189–212 (1881).
[33]D. B. Murray and L. Saviot, "Phonons in an inhomogeneous continuum: Vibrations of an embedded nanoparticle," Phys. Rev. B **69**(9), 094305 (2004).
[34]A. C. Eringen and E. S. Suhubi, *Elastodynamics* (Academic, New York, 1975).
[35]A. Tanaka, S. Onari, and T. Arai, "Erratum: Low-frequency Raman scattering from CdS microcrystals embedded in a germanium dioxide glass matrix [Phys. Rev. B 47, 1237 (1993)]," Phys. Rev. B **56**(15), 9977 (1997).
[36]H. N. Ritland, "Relation between refractive index and density of a glass at constant temperature," J. Am. Ceram. Soc. **38**(2), 86–88 (1955).
[37]C. Z. Tan and J. Arndt, "The mean polarizability and density of glasses," Physica B **229**(3), 217–224 (1997).
[38]H. N. Ritland, "Density phenomena in the transformation range of a borosilicate crown glass," J. Am. Ceram. Soc. **37**(8), 370–377 (1954).
[39]L. Su and A. Y. Yi, "Finite element calculation of refractive index in optical glass undergoing viscous relaxation and analysis of the effects of cooling rate and material properties," Int. J. Appl. Glass Sci. **3**(3), 263–274 (2012).